Resolving Convection in a Global Hypohydrostatic Model

by S. T. Garner[1], D. M. W. Frierson[2], I. M. Held[1], O. Pauluis[3], G. K. Vallis[4]

[1]Geophysical Fluid Dynamics Laboratory/NOAA, Princeton, NJ
[2]Department of Geophysical Sciences, University of Chicago, Chicago, IL
[3]Courant Institute of Mathematical Sciences, NYU, New York, NY
[4]Atmospheric and Oceanic Sciences Program, Princeton Univ., Princeton, NJ

corresponding author email address: steve.garner@noaa.gov

Abstract

Convection cannot be explicitly resolved in general circulation models given their typical grid size of 50km or larger. However, by multiplying the vertical acceleration in the equation of motion by a constant larger than unity, the horizontal scale of convection can be increased at will, without necessarily affecting the larger-scale flow. The resulting hypohydrostatic system has been recognized for some time as a way to improve numerical stability on grids that cannot well resolve nonhydrostatic gravity waves. More recent studies have explored its potential for better representing convection in relatively coarse models.

The recent studies have tested the rescaling idea in the context of regional models. Here we present global aquaplanet simulations with a low-resolution, nonhydrostatic model free of convective parameterization, and describe the effect on the global climate of very large rescaling of the vertical acceleration. As the convection expands to resolved scales, we find a deepening of the troposphere, a weakening of the Hadley cell and a moistening of the lower troposphere, compared to solutions in which the moist convection is essentially hydrostatic. The growth rate of convective instability is reduced and the convective lifecycle is lengthened relative to synoptic phenomena. This problematic side-effect is noted in earlier studies and examined further here.

1. Introduction

Length and time scales of moist convection are well separated from those of baroclinic eddies in the Earth's atmosphere. These are the two scales at which the zonally asymmetric circulation receives most of its energy. Although intermediate scales have a big effect on forecast skill, as it is traditionally defined, they may be less important in determining the climate. To the extent that this is true, the awkwardness that the huge scale separation creates for numerical climate modeling might be safely removed by effectively collapsing the mesoscale through a rescaling of the physical parameters. The ideal alteration would preserve the character of the flow in both the synoptic and convective regimes. An approach suggested by Kuang et al. (2005) comes close to this ideal by preserving the synoptic regime exactly while altering the convective regime only through a lengthening of convective lifecycles relative to external and synoptic time-scales. The only change is a factor multiplying the inertial term in the vertical equation of motion. We refer to this system as hypohydrostatic.

There are two possible physical systems that reduce to the hypohydrostatic system, one of which is considered by Kuang et al. (2005) and referred to here as "small Earth". The other, which we call "deep Earth" following Pauluis et al. (2006), is described below. In these modified physical worlds, certain alterations to the external forcing are required to maintain self-similarity in the hydrostatic regime. We find that these physical analogs, while not strictly necessary for appreciating the impact of the hypohydrostatic alteration on climate, often facilitate a physical understanding of the solutions.

The idea of directly changing the equation of motion was suggested by Browning and Kreiss (1986) as a way to improve numerical stability. The specific motivation was to make the grid-scale internal waves less hydrostatic. The computational opportunities and drawbacks of the idea were later investigated by Skamarock and Klemp (1994) and Macdonald et al. (2000). All of these studies focused on internal waves or steady circulations and did not consider the existence of physical analogs or the possibility of improving the convective dynamics.

Our main motivation is to make the grid-scale convection less hydrostatic. We explore the idea using a global grid-point model with physical closures and external forcing of intermediate complexity. The numerical model is compressible and nonhydrostatic, but we run it at far too coarse a resolution to take advantage of this extra freedom without the hypohydrostatic alteration. The physical closures are adopted from Frierson et al. (2006a). Kuang et al. (2005, hereafter KBB) and Pauluis et al. (2006, hereafter PFGHV) explored hypohydrostatic rescaling in the framework of cloud-resolving models. As in those studies, we will document the direct effect of the convection on the temperature and humidity profiles. The value of the global solutions is that they include the interaction with synoptic and planetary scales. A disadvantage is that the high-resolution (ground-truth) solution is still not computationally feasible.

In our exposition, we also emphasize the fundamental self-similarities of the hydrostatic system, as it is these self-similarities that make it possible to preserve the large-scale dynamics while rescaling the convective regime. We begin with this discussion of hydrostatic self-similarity, then proceed to describe the hypohydrostatic model in section 3 and the global numerical solutions in sections 4 and 5.

2. Self-similarity in the hydrostatic limit

The type of rescaling that we are interested in is transparent to the hydrostatic dynamics governing synoptic eddies and larger phenomena, but destabilizing with respect to moist convection at sub-synoptic scales. An easy way to find such transformations is to take advantage of the self-similarity of hydrostatic systems. Consider the inviscid, nonhydrostatic Boussinesq model,

$$d(u, v)/dt = -(\partial/\partial x, \partial/\partial y)\phi - f(-v, u) \quad (1)$$

$$dw/dt = b - \partial\phi/\partial z \quad (2)$$

$$\partial u/\partial x + \partial v/\partial y + \partial w/\partial z = 0 \quad (3)$$

$$db/dt = Q, \quad (4)$$

with standard meteorological notation. We let f_0 be a scale for the Coriolis frequency f and name three other scales, one for height $z \sim H$, one for horizontal distance, $(x, y) \sim L$ and one for horizontal velocity, $(u, v) \sim U$. Then we derive the scales $\phi \sim U^2$ and $b \sim U^2/H$ for the pressure and buoyancy, respectively, $w \sim UH/L$ for the vertical velocity, and $t \sim L/U$ for time. When the variables are normalized by these scales, the resulting nondimensional system is

$$d(\tilde{u}, \tilde{v})/d\tilde{t} = -(\partial/\partial\tilde{x}, \partial/\partial\tilde{y})\tilde{\phi} - s(-\tilde{v}, \tilde{u}) \quad (5)$$

$$r^2 d\tilde{w}/d\tilde{t} = \tilde{b} - \partial\tilde{\phi}/\partial\tilde{z}. \quad (6)$$

$$\partial\tilde{u}/\partial\tilde{x} + \partial\tilde{v}/\partial\tilde{y} + \partial\tilde{w}/\partial\tilde{z} = 0 \quad (7)$$

$$d\tilde{b}/d\tilde{t} = \tilde{Q}, \quad (8)$$

Here $d/d\tilde{t} = \partial/\partial\tilde{t} + \tilde{u}\partial/\partial\tilde{x} + \tilde{v}\partial/\partial\tilde{y} + \tilde{w}\partial/\partial\tilde{z}$ and the tilde denotes dimensionless variables: for example, $\tilde{\phi} = \phi/U^2$. There are only two parameters: $r \equiv H/L$ and $s \equiv f_0 L/U$.

The hydrostatic Boussinesq system is obtained by deleting the inertial term in (2) or (6), which is appropriate when the aspect ratio r is very small. Since this also removes the dependence on H (except as it is implicit in $\tilde{Q}$, which we return to in section 3), the hydrostatic limit is self-similar with respect to changes in H. The hydrostatic system with $Q = 0$ is also self-similar with respect to L, except for the dependence of s on L. However, it is not necessary to delete the Coriolis terms in this case. KBB showed that, for any factor γ, the additional change $f \to f\gamma$ completes the self-similarity starting from $(x, y, t) \to (x, y, t)/\gamma$ and $w \to w/\gamma$.

If z is stretched in the dimensional hydrostatic system, the follow-on changes required for similarity can be deduced from the way the above derived scales depend on H. Thus, if we change $z \to \alpha z$, the dimensionless parameter α can be removed from the dimensional system -- showing self-similarity once again -- if we simultaneously change $w \to \alpha w$ and $b \to b/\alpha$. Note that the vertical buoyancy gradient then obeys $N^2 = -(d_h b/dt)/w \to N^2/\alpha^2$, where d_h/dt is the derivative following the horizontal motion. This preserves time-scales for hydrostatic gravity waves and linearized hydrostatic convection, since the relevant dispersion relation is $\omega^2 = N^2(K/m)^2$ and the transformation implies $m \to m/\alpha$ for the vertical wavenumber. In the KBB alternative, the rescaling affects the frequency ω and the horizontal wavenumber K. The Richardson number, N^2H^2/U^2, is also invariant in deep Earth, as are all bulk parameters associated with the hydrostatic system.

To move nonhydrostatic convection closer to synoptic scales without directly affecting those larger scales, one simply chooses α and H large enough to make deep circulations isotropic in the normally hydrostatic range of the mesoscale. Of course, the numerical model has to resolve that range in order for the approach to be useful. The equivalent alternative suggested by KBB is to move the synoptic regime closer to the convective scale. Since the Rossby number, $\mathrm{Ro} = s^{-1}$, is invariant under the transformation involving L and f, choosing $\gamma > 1$ shrinks the minimum scale of the synoptic regime.

3. Implications for non-Boussinesq and forced systems

Non-Boussinesq systems include the additional dimensional parameter g, the gravitational constant. Gravity provides an external scale for H, namely the pressure scale-height, $H_p = RT/g$, where R is the gas constant and T is the temperature. The simplest extension of the vertically rescaled system involves the transformation $g \to g/\alpha$. Then the pressure scale height, which appears in the statement of hydrostatic balance in the form $\partial p/\partial z = -p/H_p$, satisfies the similarity requirement for vertical distances without rescaling T. Based on this external scale, the vertically stretched system has been termed "deep Earth" (PFGHV). The horizontally rescaled system described by KBB may be termed "small Earth" based on the identification, $L = a$, where a is the Earth's radius.

The scale for the buoyancy forcing, Q, is $U^3/(HL)$. A decrease in L therefore requires an "acceleration" of the forcing, as discussed by KBB in connection with the small-Earth system. This complication is due to the shortening of the advective time-scale and its independence from the forcing time-scale. Now for the deep-Earth system, there is no change in L. Furthermore, the factor of H^{-1} is absorbed by the change in the factor of g present in the definition of buoyancy. Nevertheless, deep Earth also requires a forcing adjustment: stretching the vertical axis reduces the radiative flux convergence and divergence and changes the associated heating and cooling rates. The adjustment can be applied directly to the external heat source and sink, as in KBB. It can also take the form of a reduction in density and total pressure via $\rho \to \rho/\alpha$ and $p \to p/\alpha$. The latter choice reduces the volumetric heat capacity, ρc_p, but preserves the equation of state without rescaling the gas constant or the temperature. It reduces the total mass of the atmosphere in the small-Earth scenario, but preserves mass in the deep-Earth atmosphere.

The potential temperature is also unaffected by the density and pressure rescaling. To preserve the specific humidity and virtual temperature, the saturation vapor pressure must change with the total pressure, as noted in the Appendix. The term "forcing" is meant to include surface fluxes and microphysics as well as radiation. The Appendix considers adjustments in all of these parts of the model physics.

4. The hypohydrostatic model

When the deep-Earth transformation of z, w and b given at the end of section 2 is applied to the dimensional Boussinesq equations, (2) becomes

$$\alpha^2\frac{dw'}{dt'} = b' - \frac{\partial\phi'}{\partial z'}. \tag{9}$$

This equation is written in terms of the original variables, denoted with primes: for example, for $z \to \alpha z$, we have written $z = \alpha z'$. Except for the primes, the other 3 equations in (1) - (4) are unchanged if Q is rescaled as just described. This is the hypohydrostatic system. In the following we refer to it without the primes. Exactly the same system arises in the small-Earth scenario after transforming x, y, t, w, f and Q as detailed in the previous section (with α instead of γ).

Rather than thinking of the factor α^2 in (9) as a discrete switch between hydrostatic ($\alpha^2 = 0$) and nonhydrostatic ($\alpha^2 = 1$) equations, as in some numerical model codes (*e.g.*, Yeh et al. 2002), we follow Browning and Kreiss (1986) in viewing it as a continuous parameter. In the case of unforced dynamics, it is equivalent to continuous changes in the gravitational constant or the Earth's radius and rotation rate. In this study, we are only interested in the hypohydrostatic case, $\alpha > 1$. The case $\alpha < 1$ would be hyperhydrostatic. The distinction between the small-g world with stretched z and the rescaled system based on (10) is analogous to the distinction between "DARE" and "RAVE" in KBB. The first approach changes parameters, whereas the second changes an equation. Macdonald et al. (2000) referred to the hypohydrostatic system as quasi-nonhydrostatic.

When $\alpha \neq 0$, the degree of hydrostasy depends on horizontal scale. Consider the growth/decay rate σ for linearized convective instability. If the static stability is $N^2 = -|N|^2$, then

$$\sigma^2 = \frac{(|N|^2/\alpha^2)\alpha^2 K^2}{\alpha^2 K^2 + m^2}, \tag{10}$$

where K is the total horizontal wavenumber and m is the vertical wavenumber (*cf.* Macdonald et al., 2000, section 3c). For $\alpha > 1$, the physical changes are equivalent to shifting the instability to larger horizontal scales -- to preserve αK -- while reducing the maximum growth rate from $|N|$ to $|N|/\alpha$.

At fixed scales K^{-1} and m^{-1}, (10) confirms that hydrostasy can always be disrupted with large enough α. We can define a coarsely resolved model as one with $K_{max} \ll m_{min}$. In such a model, or in a hydrostatic model, convection occurs at the grid scale, since this is always the most unstable scale, with $\sigma \approx |N| K_{max}/m_{min}$. However, in linearized nonhydrostatic convection, (10) applies, and some of the horizontal scale sensitivity is removed by the upper bound $\sigma_{max} = \alpha^{-1}|N|$. By choosing $\alpha \gg m_{min}/K_{max}$, one can capture this property of nonhydrostatic convection without having to increase model resolution. The effect is to destabilize a range of resolved scales and, in principle, to allow more realistic convective dynamics. In section 2, we interpreted this as moving the nonhydrostatic regime into the resolved range, closer to the synoptic regime.

Our purpose in using large α is to compensate for a horizontal grid that is much coarser than the cloud-resolving scale. This compares to the strategy of Macdonald et al. (2000) for maintaining numerical stability, which is to impose $\Delta x/\alpha \approx \Delta z$, where Δx and Δz are the horizontal and vertical grid lengths. The idea is that for fixed Δz, α should increase with Δx. The suite of convection experiments in PFGHV also maintains $\Delta x/\alpha$, starting from a cloud-resolving control case. The main reason for not following this strategy here is, of course, that a cloud-resolving global grid with $\alpha \approx 1$ is not computationally feasible. Instead we will look at sensitivity to α on a fixed grid.

Note that the transition from differential equations to difference equations has introduced Δx and Δz as parameters. The time-scale Δt has also become a parameter. For hydrostatic self-similarity in the difference equations, these intervals must scale with x, z and t, respectively. If changes in Δx are viewed as a horizontal rescaling, it is immediately clear from the small-Earth perspective that the impact of a coarse grid can be softened by introducing α into the nonhydrostatic system, as this is equivalent to a reverse horizontal rescaling. The strategy can be seen as trying to extend similarity to the nonhydrostatic equations.

Typically, the compensation is incomplete and non-similar solutions result because: (1) similarity requires all external horizontal scales, including the Earth's radius in the case of a global model and the domain size in the case of a Cartesian one, to vary with Δx, and (2) similarity also requires forcing time-scales to vary inversely with Δx, as implied in section 3. Let us refer to $\alpha H / \Delta x$ as the effective aspect ratio of the numerical experiment. If the above two conditions were met, all nonhydrostatic solutions with the same effective aspect ratio would be formally similar. This would also be true if H and Δz were varied instead of L and Δx. The approach of PFGHV can be interpreted as maintaining the effective aspect ratio and then measuring the impact of the remaining non-similarity. They emphasized a slow-down of the convective lifecycles relative to the forcing (and to the hydrometeor fall times) as the most significant non-similarity, corresponding to the second of the two requirements just named.

In small Earth, nonhydrostatic convection does not slow down, but rather synoptic phenomena speed up. However, convection does slow down in deep Earth. Let $\delta\theta$ denote the potential temperature excess of a lifted parcel. Except for unknown climate impacts on $\delta\theta$, the convective available potential energy per unit mass, $\mathrm{CAPE} \sim gH(\delta\theta)/\theta_0$, is invariant with respect to the vertical rescaling. This means that the nonhydrostatic vertical velocity, which scales as the square root of CAPE, is insensitive to the depth of the atmosphere. On the other hand, the typical duration of the convection is $\tau_C \sim H/w \sim \sqrt{\theta_0 H/(g\delta\theta)}$. This scale τ_C is the analog of $1/|N|$ in the linearized convection discussed at the beginning of the section. Just as $|N|^{-1}$ varies directly with α in the hypohydrostatic system, τ_C is proportional to H in a weak-gravity, deep-Earth system. This implies a lengthening of the convective lifecycles.

In the hypohydrostatic model, convective updraft and downdraft speeds fall off with increasing α. PFGHV characterized this result as a reaction to the increased inertia of the vertical motion. Thus, if we write CAPE $= w_C^2$, the nonhydrostatic scale for the vertical velocity is $w_{nh} \sim w_C/\alpha$, compared to $w_h \sim w_C r$ for the hydrostatic scale. The transition to nonhydrostasy occurs when $r \sim \alpha^{-1}$, which implies larger horizontal scales for larger α, as we have already noted. Because of the sensitivity of w_{nh} to α in the hypohydrostatic system, the overturning time, $\tau_C = H/w_{nh}$, is the same as in deep Earth with H increased by a factor of α. Unfortunately, longer convective lifecycles are an enormous complication, as they can create or modify interactions with dynamical, physical and numerical processes.

Sluggish convection does not necessarily mean less penetrative convection. Overshooting in a hypohydrostatic solution should scale as $\delta \sim w/(N_s/\alpha)$, where N_s is a scale for the stratification above the level of neutral buoyancy. This is simply the vertical velocity divided the frequency of a stable oscillation in the hypohydrostatic model. Thus, for nonhydrostatic convection, $\delta \sim w_C/N_s$, and this is independent of α. Nor is slower convection necessarily more entraining. If the relevant eddy velocity and mixing length that determine the diffusivity, ν, scale as w_{nh} and H, respectively, the Reynolds number, $\mathrm{Re} = w_{nh}H/\nu$ is insensitive to α. However, the results in the next section suggest a significant sensitivity to numerical diffusion acting in the horizontal.

5. A hypohydrostatic general circulation model

To explore the hypohydrostatic system in detail, we modify the dynamical core of a global nonhydrostatic grid-point model coupled to simplified moisture, radiation, and surface physics. The dynamical core is the nonhydrostatic regional atmospheric model developed within the Flexible Modeling System at GFDL (Pauluis and Garner 2006). It is the same as used by PFGHV.

The modification consists of multiplying the vertical acceleration by α^2. All runs are at a resolution of 2.0 deg latitude by 2.5 deg longitude. The vertical grid is stretched so that the spacing between levels increases from 50 m at the bottom to 500 m at the top of the domain. There are 44 levels. The atmospheric model is coupled to a slab ocean model with the intention of allowing the climate more freedom to respond to α than a configuration with fixed surface temperature. There are no continents.

The 2-degree resolution is so coarse that extremely large α is required to make even the gridscale nonhydrostatic. We realize that such drastic rescaling is not the intended practical application of the hypohydrostatic model. As discussed in KBB, the intention is to use modest rescaling (perhaps 3 to 10) to improve the convective dynamics of a high-resolution, but non-cloud-resolving, global model. However, we think it is important to see the effects of drastic rescaling in a low-resolution model in order to become familiar with some of the implications of hypohydrostatic modeling.

a) Model equations and parameterizations

The atmospheric model variables are the velocity $\boldsymbol{V} = (u, v, w)$, the potential temperature θ, the specific humidity q and the Exner function π. The equations are given in the Appendix. We integrate them on a C-grid with leap-frog time stepping for advection and physics and a split-explicit adjustment step for acoustic-gravity waves (Skamarock and Klemp, 1992). Horizontal advection is based on second-order centered differences, while vertical advection is based on the piecewise parabolic method (Collela and Woodward, 1984). There are five numerical filters: 1) fourth-order horizontal diffusion, 2) Rayleigh/Newtonian damping of the small scales near the upper boundary, 3) divergence damping of the acoustic waves, 4) Robert time filtering to stabilize the leap-frog scheme and 5) polar filtering.

The physical parameterization schemes are described in detail in the Appendix, as well as in Frierson et al. (2006a), and merely summarized here. We have chosen schemes of intermediate complexity so that transformations of the physical world associated with α can be easily catalogued and understood. Surface fluxes are obtained from a simplified Monin-Obukhov scheme in which the drag coefficient is set to a constant for unstable surface layers. There is a diffusive boundary layer with time-varying depth. The condensation scheme converts water vapor directly to rain whenever the specific humidity exceeds the saturation value (over liquid). There are no clouds. Rain is allowed to re-evaporate into subsaturated layers below the level of condensation. After each timestep, re-evaporation proceeds downward in successive layers until the condensate is used up or the layer becomes saturated. We use a gray, two-stream, radiative transfer scheme with a specified infrared absorber distribution. Incoming short-wave radiation is a function of latitude but not season or time of day. Only the surface absorbs short-wave radiation. Water vapor has no effect on either shortwave or longwave transfer (and recall that clouds are non-existent). The global slab ocean has constant, uniform heat capacity and albedo.

The more detailed description of these schemes in the appendix is accompanied by a derivation of the transformations of physical parameters equivalent to the introduction of α in the vertical equation of motion. The exercise generates the full set of nondimensional parameters that must be held invariant during the vertical or horizontal rescaling in order to preserve the hydrostatic sub-system. We reiterate that this is done for its interpretive value, but that the model is defined directly by the alterations made in (9) or (A3).

Our mixed-layer heat capacity is given a small value in order to shorten the spin-up time to around 18 months. Starting from a spun-up solution, we have used 6 months for re-equilibration with each new α. With radiation unaffected by clouds and water vapor, the zonal-mean surface temperatures are quite insensitive to the rescalings, showing less than 1K variation between experiments. The model climatologies presented here are averages over one year following equilibration. This leaves an acceptable amount of sampling error in the form of inter-hemispheric and longitudinal asymmetry.

We have obtained climatologies for $\alpha = 1$, 100, 200 and 300. As suggested above, the large gap between the first two values is required by the coarse model resolution. Since the horizontal grid length is around $\Delta x = 250$ km in the Tropics, the aspect ratio of the convection at the smallest resolved scale is around 1:25. Therefore, nonhydrostatic effects cannot be expected until at least $\alpha \approx 25$ (for an effective aspect ratio of order unity). It turns out that the grid scale is still favored by the convection well beyond this value -- up to $\alpha \approx 50$. This seems to be the threshold for significantly nonhydrostatic convection. The real-world setting $\alpha = 1$ is dynamically indistinguishable from $\alpha = 0$ on our 2-by-2.5-deg grid: the control solution is essentially hydrostatic.

b) Impact on the convective scale

A direct impression of the impact of hypohydrostasy can be found in the field of precipitation. The plots in Fig. 1 are of instantaneous rain rate in the equilibrated solutions with $\alpha = 1$ and $\alpha = 300$. The grid scale in the second case corresponds to an effective aspect ratio of $\alpha H / \Delta x \approx 12$. (In the deep-Earth analog, where g is reduced by a factor or 300, the tropopause height is on the order of 3000 km, or about 12 times the grid length.) The plot shows that in the Tropics, individual storms in the large-α case vary in size from 2 to 8 grid points (500 km to 2000 km), compared to 1 grid point in the control. Therefore the effective aspect ratio falls to near unity for the largest storms. There is some expansion of the clear regions, but the typical gap is much less sensitive to α than the size of the convection. There is also some expansion of the frontal and warm-sector convection in the extratropical eddies. However, despite the enormous rescaling, the precipitation in the Extratropics is only a small amount lighter than in the control.

Shown in Fig. 2 is the cross section of vertical velocity along the Equator at exactly the same time as the precipitation plots. The contrast in horizontal scale between the two solutions mirrors that of the tropical precipitation fields. One also notices that the convection is deeper in the large-α case. The height of the deepest updrafts increases from around 12 km to around 15 km. As we will see shortly, this is not explained by the small difference in tropopause height. It is due to an increase in the overshooting distance for large α, something that is not predicted by the scaling argument outlined at the end of section 4. The most likely explanation is that narrower updrafts are more vulnerable to numerical diffusion -- a process that is sensitive to the fixed horizontal grid length rather than to α directly. Indeed, within the large-α solution, the least penetrative updrafts are the narrowest updrafts. In examining the time-dependent solution, we noticed that most of the gravity-wave activity in the stratosphere is due to the narrow updrafts. This is presumably because a slower penetration rate (the vertical velocity in the large-α case is about one-third that of the control) excites the hydrostatic waves more weakly. The frequencies of the nonhydrostatic waves scale with w, but nonhydrostatic waves are more laterally dispersive and generally less prominent than hydrostatic waves in the stratosphere.

We also examine the zonal wavenumber spectra of vertical velocity, shown in Fig. 3. For this calculation, the velocities were sampled at a height of 5.0 km along the equator and 40 deg North and South latitude every 3 hours for the full 12 months of the simulations. Each spectrum is normalized by the square root of the variance for that particular run and latitude. The hypohydrostatic transformation shifts power to the larger zonal scales in both the Tropics and midlatitudes. In the midlatitudes, the synoptic eddy scale grows more active at the expense of the mesoscale. However, we show in the next subsection that the total eddy kinetic energy is not sensitive to α outside the Tropics. In the Tropics, the control solution appears underdiffused in the sense that the power increases (slightly) towards smaller scales. However, rather than indicating underdiffusion of a turbulent cascade, this pattern arises from the “ultraviolet catastrophe” (no growth-rate bound at small scales) that characterizes hydrostatic convection. For larger α, this feature disappears as power spreads to larger scales. By $\alpha = 300$, there may be a slightly shallower spectral slope between wavenumbers 36 and 9 (half-wavelengths between 2 and 8 gridpoints).

c) Impact on the zonal-mean circulation

The zonal-mean circulation and moisture fields for our control case are shown in Fig. 4. The zonal wind is qualitatively similar to that of the present-day Earth, with the exception of the polar stratospheric jets, which are missing. Also, the tropical easterlies are too strong. These excessive trade winds are directly related to an unrealistically strong Hadley cell, which can be seen in the plot of mean meridional circulation. The specific humidity in the tropical lower troposphere is about 10 percent dryer than observed. A more thorough discussion of the zonal-mean climate, including the eddy energy and energy transports, can be found in Frierson et al. (2006a, 2006b). Their model couples the same physics schemes with a spectral hydrostatic dynamical core. However, the resulting climate differs only slightly and we can safely assume the differences are due to the change to a finite-difference core rather than to nonhydrostatic equations.

Zonal-mean difference fields between $\alpha = 1$ and $\alpha = 300$ are plotted in Fig. 5. There are four main structural differences. First, the negative perturbation in the zonal wind field near latitude 20 deg indicates a weakening of the subtropical jet when α is increased. This is related to the second difference, the weaker Hadley cell indicated by the meridional streamfunction. The negative perturbation in the temperature near 14 km altitude shows the upward shift of the tropopause in the large-α solution, primarily in the extratropics. Finally, the specific humidity is greater by almost 2 g/kg just above cloud base in the Tropics. The graph of surface zonal-mean winds in Fig. 6 shows the weakening of the trade winds with increasing α. There is still considerable sampling error in the subpolar easterlies in our one-year simulation.

The lifting of the tropopause is likely a direct result of the deeper penetration of the convection in the hypohydrostatic case. The rise is more subtle than the deepening of the convection itself. As we saw in Fig. 2, the latter amounts to around 3 km, whereas the tropopause is raised by less than 1 km. The weakening of the Hadley cell is much less drastic than the change in vertical motion within convective elements. The latter is close to a factor of 3, as seen in Fig. 2. To conserve mass, the typical spatial and temporal gaps between individual updrafts has to have decreased relative to the size and lifetime of the convection (*e.g.*, Robe and Emanuel 1996).

The weaker Hadley cell is associated with considerably less latent heating in the deep Tropics, as seen in the zonal-mean heating distributions in Fig. 7. The time-mean latent heating rate at the equator decreases monotonically from 610 W/m^2 to 370 W/m^2 (21 to 13 mm/day in corresponding units of precipitation rate) between $\alpha = 1$ and $\alpha = 300$. Outside the Tropics, the precipitation is less sensitive to α. At ± 35 deg, the time-mean latent heating rate decreases monotonically from 150 W/m^2 to 135 W/m^2, a 10 percent variation.

Although the tropopause is lifted discernibly, the difference fields, for the most part, show that the circulation outside the Tropics is weakly affected by α. A further measure of this insensitivity is the root-mean-squared horizontal windspeed in the extratropical storm tracks. Values of RMS eddy wind amplitude sampled at its maximum level of 7.2 km and at latitude $\pm 40°$ are listed in the first row of Table 1. The variation is not significant since it is comparable to the interhemispheric variation (not shown).

Table 1 also shows the variation in upper-tropospheric vertical velocity as a function of the rescaling parameter. The values listed are the maximum positive w at 10.3 km over a 6-deg band centered on the equator during the final 6 months of the integrations. The nonhydrostatic results have a weaker dependence on α than in the scaling law, $w_{nh} \sim \alpha^{-1} w_C$, derived in section 3. This derivation assumed non-varying convective potential energy and non-entraining updrafts. If we use the case $\alpha = 200$ for a numerical reference, we have $w_{nh} = \alpha^{-1}(70\text{ m/s})$. This function, $w_{nh}(\alpha)$, is evaluated in the Table for comparison to the model result. Recall that the scaling for hydrostatic convection is $w_h \sim r w_C$. Since $r = 1/25$ for gridscale convection, the model result, $w_h \approx 1.4\text{ m/s}$, fixes the control solution numerically at $w_h = r(35\text{ m/s})$. This value is also recorded in the Table. The two scaling laws intersect when $\alpha = 2/r = 50$. As mentioned in section 5a, we first noticed nonhydrostatic behavior in the tropical convection near this value of the rescaling parameter. Matching the two scaling laws gives a reasonable estimate of the threshold.

Cumulus parameterizations are used in general circulation models to improve the precipitation distribution as well as the vertical profiles of temperature, humidity and cloud water. In Fig. 8 we show the time-mean temperature and specific humidity profiles for the entire Tropics between 20 deg South and 20 deg North. There is a slight monotonic cooling of the middle troposphere as we progress from the control solution to $\alpha = 300$. For overall radiative balance, there is a commensurate warming in the extratropics (not shown). The cooling may simply be a result of a slower convective overturning that is not fully offset by the frequency of convection or a reduction in local radiative cooling. At the same time, the layer extending from cloud base at 1 km to about 4 km becomes systematically moister, apparently as a result of enhanced shallow convection. The biggest temperature change occurs at 5 km and approaches 1 deg, while the moistening peaks near 2 km with a value of just under 2 g/kg. These changes can also be seen in Fig. 4.

6. Discussion

The global experiments confirm the low impact of the rescaling on extratropical dynamics. Although we do see modest changes in the spectrum of vertical velocity, the impact on eddy kinetic energy is small. The extratropical tropopause is also raised significantly, suggesting that nonhydrostatic convection is of some relevance for the maintenance of the extratropical tropopause in this model (consistent with the results of Frierson et al. 2006a). The larger horizontal scale and deeper penetration of the tropical convection suggest that the hypohydrostatic model is less sensitive to horizontal diffusion, hence to horizontal resolution.

There is also sensitivity in the vertical profiles of tropical temperature and humidity. In the control run, these profiles show biases similar to those of cloud-resolving models run at coarse resolutions (*e.g.*, PFGHV and references therein). Our most drastically rescaled solution shows changes in the profiles that are of the right size and shape to be seen as significant corrections of those biases. It is not clear how much of this match is coincidental, since we do not have the converged global climatology for comparison.

Several of the effects from hypohydrostasy are qualitatively similar to changes resulting from the incorporation of a simple convection scheme. Both hypohydrostasy and a simple convection scheme (e.g., Frierson 2006) yield a larger scale of vertical motion and precipitation, a weakened Hadley circulation, reduced equatorial precipitation, and deeper penetration of convection. The moistening of the tropical lower troposphere also qualitatively reproduces the effect of parameterized shallow convection.

The lower-tropospheric drying in coarse models is due to suppressed shallow convection, while the mid-tropospheric warming probably results from the unrealistically fast subsidence associated with hydrostatic convection. Hypohydrostatic rescaling promotes shallow convection and lower-tropospheric moistening by directly compensating for the low resolution. Shallow, non-precipitating convection in nature plays a qualitatively similar role, even though it is at least an order of magnitude narrower than in either the referenced cloud-resolving experiments or the rescaled global experiments. The rescaling cools the middle troposphere by slowing down the overturning compared to radiative and surface forcing time-scales. Part of the slow-down comes from realistic nonhydrostatic dynamics (*e.g.*, Pauluis and Garner 2006), but the rest is due to the aforementioned rescaling artifact that has no natural analog.

The cloud-resolving model (CRM) experiments of PFGHV show that increasing α corrects only about half the coarse-resolution temperature bias and that, even at just twice the control resolution, *i.e.*, at $\Delta x = 4$ km, it makes the lower-tropospheric humidity bias worse than $\alpha = 1$. It is not immediately clear how to reconcile this result with the global experiments, but we can offer some preliminary ideas. The effective aspect ratio of the CRM suite is $\alpha H / \Delta x = 5$, comparable to that of our marginally nonhydrostatic solution ($\alpha = 100$), which has $\alpha H / \Delta x = 4$. using $H = 10$ km in both cases. However, our radiative and boundary-layer forcings are effectively much stronger. Let us assume that the Earth's rotation and curvature are not directly relevant in the global-model Tropics and that the domain size is not relevant in the cloud-resolving model. Then the non-similarity is due to the fact that our scaled forcing is stronger by a factor of about 125 (the ratio of the grid sizes) or, equivalently, that our convection is 125 times slower than in the CRM solution. Shallow convection is not directly driven by the tropospheric radiative cooling and may be unresponsive to relative changes in radiative forcing. However, deep convection is sensitive to this forcing and takes up a larger fraction of time and space in the rescaled global model. As a result, it may have an exaggerated importance in controlling lower-tropospheric humidity.

The comparison between the global and cloud-resolving experiments is complicated by the use of simplified precipitation, radiation and boundary-layer physics in the former. The precipitation fall time is much closer to a convective lifetime in the CRM solutions and therefore a possible source of sensitivity as the convection slows down. The surface fluxes in our solutions are damped by the slab ocean, which cools beneath strong convection. Also, potentially important radiative feedbacks are eliminated in the global model by the reliance on specified absorbers.

7. Conclusion

Hypohydrostatic modeling was once suggested as a way to improve numerical stability by energizing nonhydrostatic internal waves. It may also be a good way to promote more realistic convection and thereby possibly reduce the dependence of numerical models on cumulus schemes, as proposed by Kuang et al. (2005). By increasing the horizontal scale of convection, clouds and vertical motion become resolved and the transfer of heat and momentum can be calculated explicitly at scales larger than the model grid. The solution in a model with $\alpha > 1$ would converge at a coarser resolution than in a model with $\alpha = 1$.

An important step in evaluating this approach to cumulus parameterization is to see how the altered convection interacts with synoptic and planetary scales, as we have sought to do here. The relatively coarse resolution.keeps us from knowing how close our solutions are to converging or indeed whether the hypohydrostatic model improves the representation of convection. However, we were able to explore some of the basic properties of the rescaling in a global context. The computations are complementary to the high-resolution, convection-resolving simulations of KBB and PFGHV.

The insensitivity to α outside the Tropics is a consequence of the robustness of hydrostatic balance in mid-latitudes, where hydrostasy is maintained not only by the small aspect ratio of the flow but also by the inhibition of vertical motion by rotation and stratification. We find that even with values of α as large as 300, large-scale midlatitude dynamics were little altered, although the sensitivity of the tropopause height warrants further study. This is a promising result, for it means that with the more moderate values of α that might be used in the future, the baroclinic dynamics at the deformation scale will not be adversely affected. Of course, the one-year integration time and lack of seasonal forcing prevent any assessment of the model's interseasonal or interannual variability, a key aspect of climate.

The most encouraging result of the hypohydrostatic experiments may be the qualitative similarity to the effects of a simple convection scheme, such as that used by Frierson (2006). A potential drawback to the approach is the slowing of convective growth and the lengthening of convective lifecycles. In the real atmosphere there is a significant difference between typical convective time-scales and time-scales of the larger circulation, with mesoscale systems sometimes filling the gap. If mesoscale systems were completely absent, we might suppose that artificially increasing the time-scale of convection would have little effect, so long as it did not impinge on the large scale. Our experiments suggest that this is true. However, interactions with the diurnal time-scale and radiatively active clouds are missing from our model, and would become serious complications in a more realistic GCM.

As model resolution inexorably increases, the value of α needed to expand convection beyond the grid scale will diminish. At sufficiently high resolution, perhaps with the grid scale of order 10 km or less, a value of $\alpha = 2$ or $\alpha = 3$ will suffice to resolve important aspects of the deep convection, but will at the same time be virtually undetectable to the large-scale and mesoscale circulation. It is at such resolutions that the approach may become a parameterization tool.

Appendix

We show here that the hypohydrostatic version of the general circulation model can be obtained by changing parameters of the physical system, starting from either the gravitational constant or the planetary radius. This is shown by finding a complete set of nondimensional parameters and arranging to keep them all fixed except for the one that relates the vertical and horizontal length scales (the aspect ratio). The Buckingham Pi Theorem conveniently determines when the list is complete.

We first present the equations of the dynamical core and its set of nondimensional parameters, and then consider the physical parameterizations one by one. Complementary explorations of the nondimensional parameters and extensions to other models can be found in Frierson (2005) and Pauluis et al. (2006). A complete description of the physical parameterizations used in the present study can be found in Frierson et al. (2006a). As long as the physical building blocks of a particular model are standard, the way in which they are assembled or simplified should have little or no impact on this discussion.

The hypohydrostatic model consists of the following dimensional equations:

$$\frac{\partial u}{\partial t} = -\boldsymbol{V}\cdot\nabla u + fv + \frac{uv\tan\phi}{a} - \frac{c_p\theta_v}{a\cos\phi}\frac{\partial\pi}{\partial\lambda} + D_u \qquad \text{(A1)}$$

$$\frac{\partial v}{\partial t} = -\boldsymbol{V}\cdot\nabla v - fu - \frac{u^2\tan\phi}{a} - \frac{c_p\theta_v}{a}\frac{\partial\pi}{\partial\phi} + D_v \qquad \text{(A2)}$$

$$\frac{\partial w}{\partial t} = -\boldsymbol{V}\cdot\nabla w - \alpha^{-2}\left(g + c_p\theta_v\frac{\partial\pi}{\partial z}\right) + D_w \qquad \text{(A3)}$$

$$\frac{\partial\pi}{\partial t} = \frac{\pi}{\mu}\left(-\frac{\nabla\cdot\pi^{\mu}\boldsymbol{V}}{\pi^{\mu}} + \theta_v^{-1}\frac{d\theta_v}{dt}\right) \qquad \text{(A4)}$$

$$\frac{\partial\theta}{\partial t} = -\boldsymbol{V}\cdot\nabla\theta + \frac{Q_R + Q_C}{c_p\pi} + D_\theta \qquad \text{(A5)}$$

$$\frac{\partial q}{\partial t} = -\boldsymbol{V}\cdot\nabla q - \frac{Q_C}{L_v} + D_q. \tag{A6}$$

Here, D represents boundary-layer tendencies, Q_R the radiative heating/cooling and Q_C the condensational heating/cooling. Longitude and latitude are denoted λ and ϕ, respectively. By definition, $\pi = (p/p_0)^{\kappa}$, where p_0 is a reference pressure and $\kappa = R_d/c_p$, and the potential temperature is related to the temperature by $\theta = T/\pi$. The specific humidity is $q = \varepsilon e/[p-(1-\varepsilon)e]$, where e is the partial pressure of water vapor with reference value e_0, and $\varepsilon = R_d/R_v$. We have written $\theta_v = \theta[1+(\varepsilon^{-1}-1)q]$ for the virtual potential temperature in (A3) and (A4). The various thermodynamic constants are: the latent heat of vaporization, L_v; the specific heats at constant pressure and volume, c_p and c_v; and the gas constants for dry air and water vapor, R_d and R_v. We have also defined $\mu = \kappa^{-1}-1$ in (A4) and let a denote the radius of the Earth in (A1) and (A2). The Coriolis parameter is defined as $f = 2\Omega\sin\phi$, with Ω the rotation frequency.

We have written the model equations in their hypohydrostatic form by including the nondimensional factor α^2 in (A3). In the following, we treat the equations as though this factor were missing, and allow it to re-emerge from changes in the physical system.

There are 6 external parameters of the dry dynamical core: a, Ω, p_0, R_d, c_p, and g, and 2 more associated with moisture: e_0 and R_v. There are 4 physical dimensions: m, s, kg and K. Hence, by the Buckingham Pi Theorem, there will be 6 + 2 - 4 = 4 independent nondimensional parameters for the dynamical core. We take these to be

$$\begin{aligned} P_1 &= R_d T_0/(ga) \\ P_2 &= \kappa \\ P_3 &= \varepsilon \\ P_4 &= e_0/p_0\,, \end{aligned} \tag{A7}$$

with $T_0 = a^2\Omega^2/c_p$, a temperature scale. The pressure scale is arbitrary except in the presence of moisture. The first parameter, P_1, can be recognized as the aspect ratio, H/L, with $H = R_d T_0 / g$ and $L = a$. Therefore, P_1^2 is a measure of nonhydrostasy. Making any other choice for H or L merely multiplies P_1 by a factor that will be held invariant in the rescaling. In particular, to define a hydrostasy parameter that is more appropriate for the forced climate system, the temperature scale will be replaced below with a radiative temperature, without changing the dependence of the hydrostasy parameter on the rescaling factor. If the equations were hydrostatic, one could convert to pressure coordinates to show that g and P_1 were redundant (Frierson 2005), just as H and r are redundant in the hydrostatic Boussinesq system discussed in the Introduction.

We are now ready to introduce the physical parameterizations one by one. There will be 4 more physical parameters with no additional units. We therefore expect 4 more nondimensional parameters.

a) Radiation, condensation and turbulence

The radiative forcing is given by

$$Q_R = \frac{R_d \theta_v}{p_0 \pi^{\mu}}\left(-\frac{\partial F}{\partial z}\right), \tag{A8}$$

where F is a linear combination of σT^4, with σ the Stefan-Boltzmann constant, and R_s, the solar constant. The introduction of two external parameters with no new dimensions adds two nondimensional parameters. The list of nondimensional parameters expands to include:

$$\begin{aligned} P_5 &= \frac{g R_s}{p_0 \Omega c_p T_{eq}} \\ P_6 &= T_{eq}/T_0 , \end{aligned} \tag{A9}$$

where $T_{eq} = (R_s/\sigma)^{1/4}$, a radiative equilibrium temperature. The first of these is a scale for the radiative forcing relative to the dynamical tendency of the specific entropy. The pressure scale-height, $H = RT_{eq}/g$, was used to scale the vertical derivative in (A8). It can also be used to identify P_6 as an inverse Burger number.

Latent heating, Q_C, brings in the latent heat of vaporization, L_v. This becomes normalized by $c_p T_{eq}$ if we equate the dynamical and physical time-scales in (A5). The list then includes:

$$P_7 = \frac{L_v}{c_p T_{eq}}. \tag{A10}$$

The actual form of the heating is

$$Q_C = -L_v (dq/dt)^*, \tag{A11}$$

where $(dq/dt)^*$ is a rate of change that depends on the dynamics and the Clausius-Clapeyron relation for the saturation vapor pressure, e_{sat}. However, the Clausius-Clapeyron relation, $e_{sat} = e_0 \exp(L_v / R_v T)$, introduces no additional parameters.

The diffusive tendencies are

$$D_\xi = \rho^{-1} \frac{\partial}{\partial z}\left(\rho K \frac{\partial \xi}{\partial z}\right). \tag{A12}$$

where $\rho = p_0 \pi^\mu / (R_d \theta_v)$ is the density and $K(z)$ is the diffusivity. At the surface, the flux $F_\xi = -\rho K \partial\xi / \partial z$ is replaced by

$$C\rho |\boldsymbol{V}(z_1)| [\xi_0 - \xi(z_1)], \tag{A13}$$

where z_1 is a level within the surface layer, ξ_0 is the boundary value and C is the drag coefficient. The profile $K(z)$ is extended upward from z_1 using a function of height and bulk Richardson number. We see from (A12) and (A13) that K scales as CUH, with U a scale for $\boldsymbol{V}$. Therefore, diffusion introduces the parameter

$$P_8 = \frac{Cga}{R_d T_{eq}}, \tag{A14}$$

where we have used $U = \Omega a$. The bulk Richardson number used to determine the K profile scales as $R_d T_{eq}/U^2$, which is not an independent parameter.

We have shortened the list of nondimensional parameters by not referring directly to Monin-Obukhov theory. This underlying theory expresses the surface flux (A13) in terms of two parameters rather than one, namely von Karman's constant and the surface roughness length z_0.

This brings the count to 8 nondimensional parameters and completes the list. It is now fairly simple to see what set of parameter changes can make the model hypohydrostatic, *i.e.*, unaltered except for the vertical acceleration term, and what physical interpretation is associated with each of these. The nonhydrostasy parameter, redefined based on the radiative temperature, is

$$r \equiv \frac{R_d T_{eq}}{ga}. \tag{A15}$$

This is the product of P_1 and P_6. We next present two methods of increasing nonhydrostasy by increasing r, namely, "deep Earth" and "small Earth". We emphasize that these are exactly, rather than asymptotically, equivalent systems.

b) Deep Earth

The deep-Earth scheme decreases gravity via $g \to g/\alpha$. To preserve P_5 in (A9) we must either decrease the reference pressure or increase the solar constant by the factor α. We arbitrarily make the first choice here and make the second choice in the small-Earth rescaling below. Then the saturation vapor pressure decreases to keep P_4 unchanged. Since the temperature scale does not change, neither does P_6 or P_7. To hold P_8 fixed, we must multiply the drag coefficient by α.

A summary of the deep-Earth rescaling is as follows:

$$\begin{aligned} g &\to g/\alpha \\ p_0 &\to p_0/\alpha \\ e_0 &\to e_0/\alpha \\ C &\to C\alpha \end{aligned} \tag{A16}$$

As intended, the effect of these changes on the full set of nondimensional parameters consists solely of $r \to r\alpha$. The consequence for the model variables involves just two transformations, namely, $z \to z\alpha$ and $w \to w\alpha$, both due to the increase in scale height, RT_{eq}/g. These two changes preserve the form of the divergence operator in (A4) and the form of the advection operator in the other 5 equations.

c) Small Earth

The small-Earth scaling decreases Earth's radius via $a \to a/\gamma$. We hold the temperature scale T_0 invariant by increasing the rotation rate and thereby fixing the velocity scale, $U = \Omega a$. In order that P_5 does not change, we amplify the radiative forcing R_s. This leads to an increase in the Stefan-Boltzmann constant, so that T_{eq} and therefore P_6 remain unchanged. As in the deep-Earth scaling, the drag coefficient must change by a factor of γ to fix P_8.

A summary of the small-Earth rescaling is as follows:

$$\begin{aligned} a &\to a/\gamma \\ \Omega &\to \Omega\gamma \\ (R_s, \sigma) &\to (R_s, \sigma)\gamma \\ C &\to C\gamma \end{aligned} \tag{A17}$$

If horizontal diffusion is used, the diffusivity ν must be decreased: for ∇^n diffusion or hyperdiffusion, $\nu \to \nu\gamma^{-n}$. The alteration of the nondimensional set is confined to $r \to r\gamma$. The transformation of the model variables consists of $(x, y, t) \to (x, y, t)/\gamma$ and $w \to w\gamma$. Note that these changes multiply the divergence and advection operators by γ, balancing an identical change in the time derivatives. The required change in the metric terms is accomplished by the first transformation in (A17).

The fact that the hypohydrostatic rescaling can be fully reproduced by changes to physical parameters not only gives us a physical intuition of the system but also assures us that all relevant conservation laws will be retained.

References

Browning, G.L., and H.-O. Kreiss, 1986: Scaling and computation of smooth atmospheric motions. *Tellus*, **38A**, 295-313.

Collela, P., and P.R. Woodward, 1984: The piecewise parabolic method (PPM) for gas-dynamical simulations. *J. Comput. Phys.*, **54**, 174-201.

Frierson, D.M.W., 2005: Studies of the general circulation with a simplified moist general circulation model. Ph.D. thesis, Princeton University, 218 pp.

Frierson, D.M.W., I.M. Held and P. Zurita-Gotor, 2006a: A gray-radiation aquaplanet moist GCM. Part I: Static stability and eddy scale. *J. Atmos. Sci.*, in press.

Frierson, D.M.W., I.M. Held and P. Zurita-Gotor, 2006b: A gray-radiation aquaplanet moist GCM. Part II: Energy transports in altered climates. Submitted to *J. Atmos. Sci.*

Frierson, D.M.W., 2006: The dynamics of idealized convection schemes and their effect on the zonally averaged tropical circulation. Submitted.

Kuang, Z, P.N. Blossey and C.S. Bretherton, 2005: A new approach for 3D cloud-resolving simulations of large-scale atmospheric circulation. *Geophys. Res. Lett.*, **32**, L02809.

Macdonald, A.E., J.L. Lee and Y. Xie, 2000: The use of quasi-nonhydrostatic models for mesoscale weather prediction. *J. Atmos. Sci.*, **57**, 2493-2517.

Pauluis, O., and S.T. Garner, 2006: Sensitivity of radiative-convective equilibrium simulations to horizontal resolution. *J. Atmos. Sci.*, **63**, 1910-1923.

Pauluis, O., D.M.W. Frierson, S.T. Garner, I.M. Held and G.K. Vallis, 2006: The hypohydrostatic rescaling and its impacts on atmospheric convection. *Theoretical and Comp. Fluid Dyn.*, to appear.

Robe, F.R., and K.A. Emanuel, 1996: Moist convective scaling: some implications from three-dimensional could ensemble simulations. *J. Atmos. Sci.*, **53**, 3265-3275.

Skamarock, W.C., and J.B. Klemp, 1992: The stability of time-split numerical methods for the hydrostatic and nonhydrostatic elastic equations. *Mon. Wea. Rev.*, **120**, 2109-2127.

Skamarock, W.C., and J.B. Klemp, 1994: Efficiency and accuracy of the Klemp-Wilhelmson time-splitting technique. *Mon. Wea. Rev.*, **122**, 2623-2630.

Yeh, K.-S., J. Cote, S. Gravel, A. Methot, A. Patoine, M. Roch and A. Staniforth, 2002: The CMC-MRB Global Environmental Multi-Scale (GEM) Model. Part III: Nonhydrostatic formulation. *Mon. Wea. Rev.*, **130**, 339-356.

Figures

Fig. 1. Instantaneous rain rate (mm/day) in solutions with $\alpha = 1$ (top) and $\alpha = 300$ (bottom).

Fig. 2. Vertical cross sections of instantaneous vertical velocity (m/s) at the Equator in the solutions with $\alpha = 1$ (top) and $\alpha = 300$ (bottom). The contour levels differ by a factor of 3 between the panels.

Fig. 3. Normalized power spectra of midtropospheric vertical velocity at the equator (left) and 40 deg latitude (right) for all four climates: $\alpha = 1$ (solid), $\alpha = 100$ (dotted), $\alpha = 200$ (dot-dashed), $\alpha = 300$ (dashed).

Fig. 4. Zonal-mean circulation and humidity from the control solution: zonal wind in m/s (upper left), temperature in K (upper right), meridional streamfunction in m^2/s (lower left) and specific humidity in g/kg (lower right).

Fig. 5. Differences in the zonal-mean circulation and moisture between $\alpha = 1$ and $\alpha = 300$: zonal wind in m/s (upper left), temperature in K (upper right), meridional streamfunction in m^2/s (lower left) and specific humidity in g/kg (lower right).

Fig. 6. Zonal-mean, time-mean surface zonal wind (m/s) in solutions with $\alpha = 1$ (solid curve) and $\alpha = 300$ (dashed).

Fig. 7. Zonal-mean, time-mean precipitation rate (W/m^2) for all four climates: $\alpha = 1$ (solid), $\alpha = 100$ (dotted), $\alpha = 200$ (dot-dashed), $\alpha = 300$ (dashed).

Fig. 8. Vertical profiles of time-mean temperature (K) and specific humidity (g/kg) averaged over the Tropics in the three hypohydrostatic solutions, plotted as a departure from the control climate: $\alpha = 100$ (dotted), $\alpha = 200$ (dot-dashed), $\alpha = 300$ (dashed).

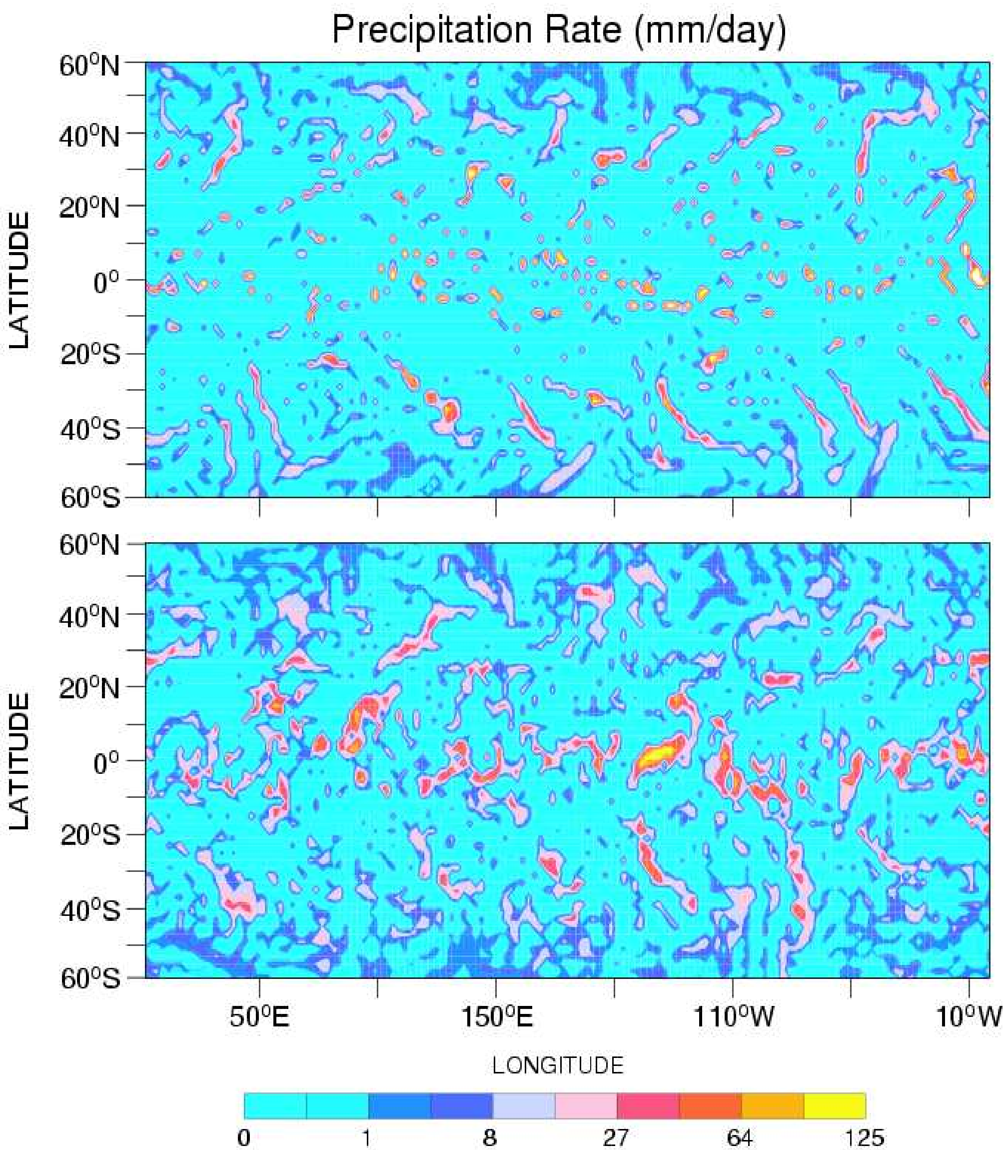

Fig. 1. Instantaneous rain rate (mm/day) in solutions with $\alpha = 1$ (top) and $\alpha = 300$ (bottom).

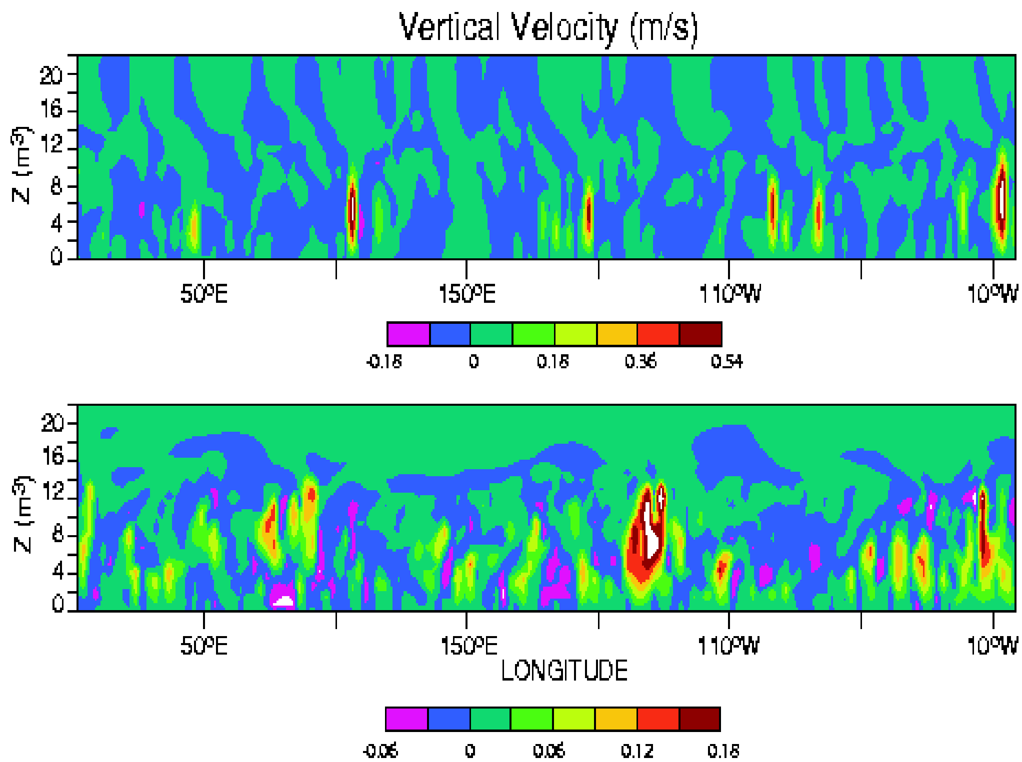

Fig. 2. Vertical cross sections of instantaneous vertical velocity (m/s) at the Equator in the solutions with $\alpha = 1$ (top) and $\alpha = 300$ (bottom). The contour levels differ by a factor of 3 between the panels.

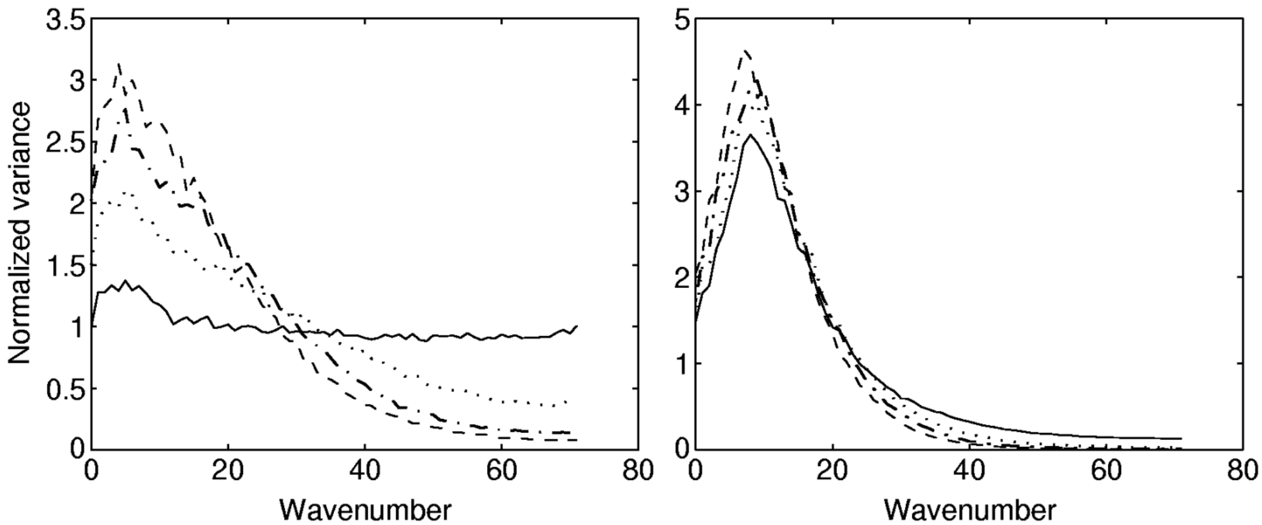

Fig. 3. Normalized power spectra of midtropospheric vertical velocity at the equator (left) and 40 deg latitude (right) for all four climates: $\alpha = 1$ (solid), $\alpha = 100$ (dotted), $\alpha = 200$ (dot-dashed), $\alpha = 300$ (dashed).

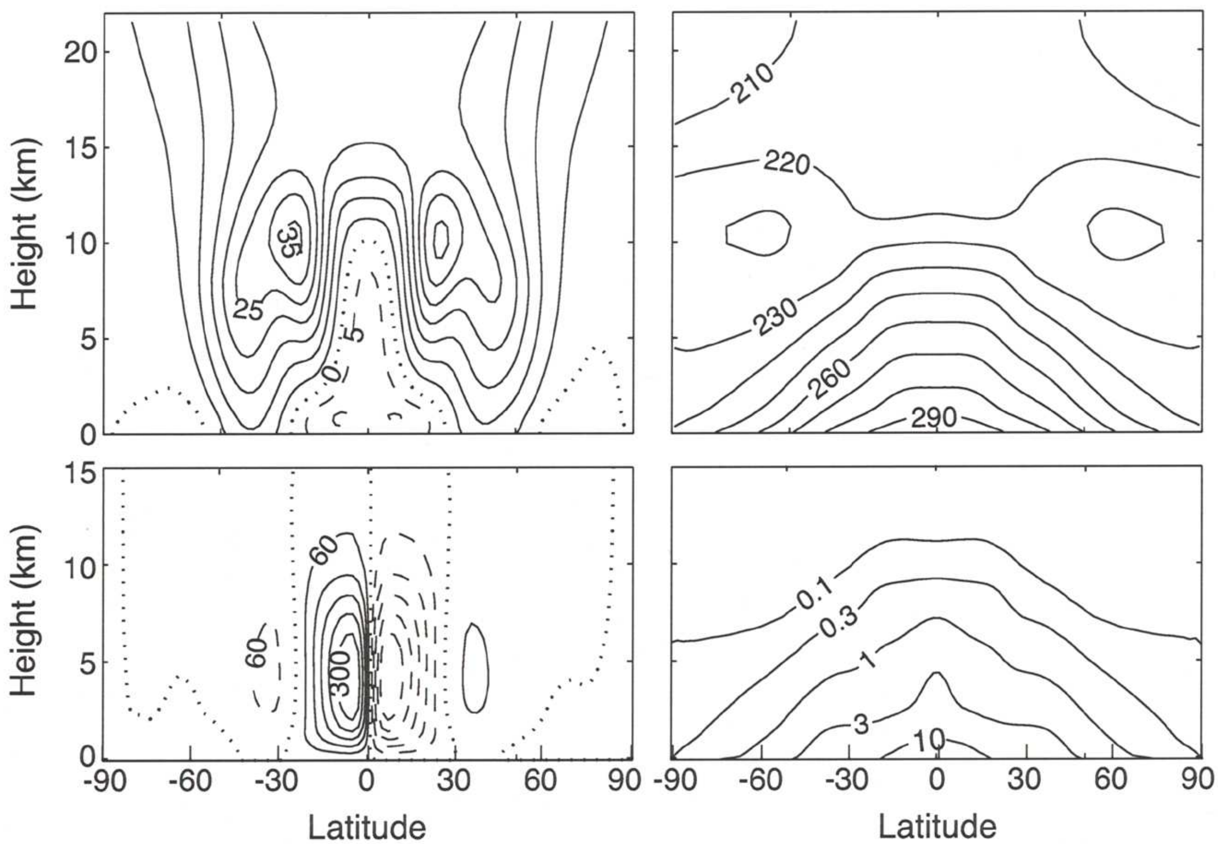

Fig. 4. Zonal-mean circulation and humidity from the control solution: zonal wind in m/s (upper left), temperature in K (upper right), meridional streamfunction in m^2/s (lower left) and specific humidity in g/kg (lower right). Contour interval is 5 m/s in the first panel.

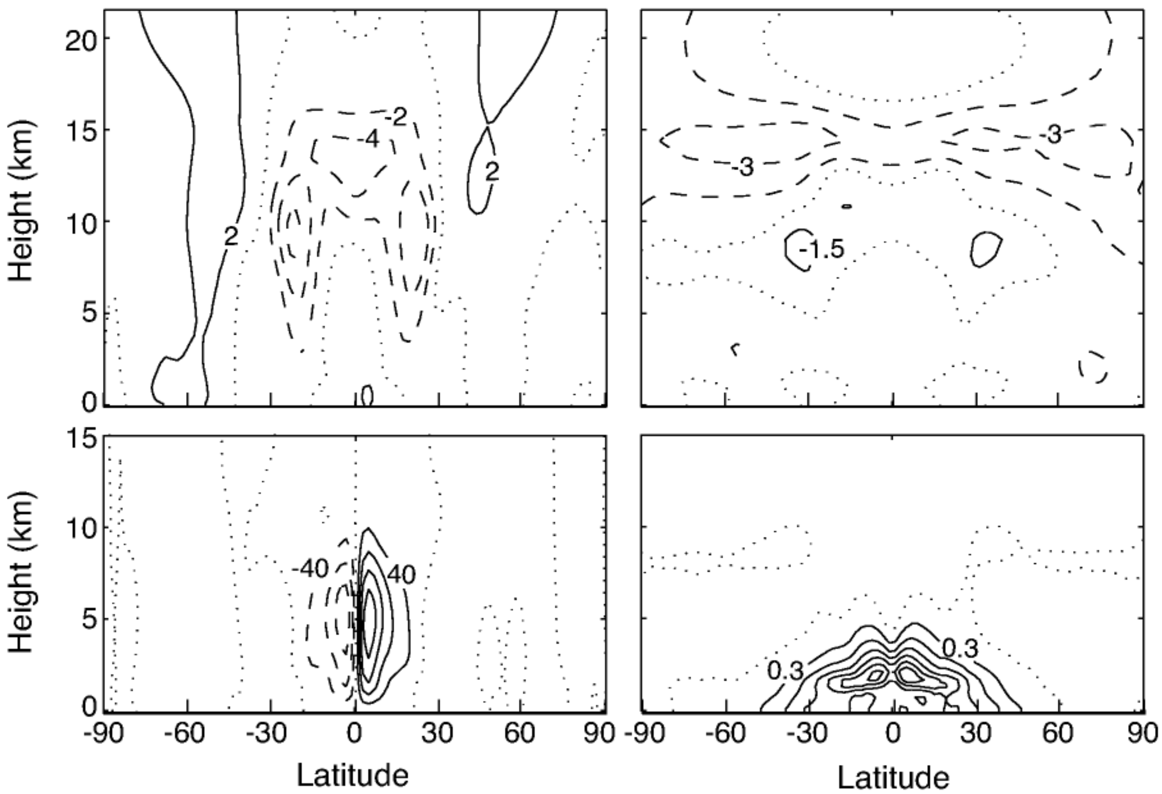

Fig. 5. Differences in the zonal-mean circulation and moisture between $\alpha = 1$ and $\alpha = 300$: zonal wind in m/s (upper left), temperature in K (upper right), meridional streamfunction in m^2/s (lower left) and specific humidity in g/kg (lower right).

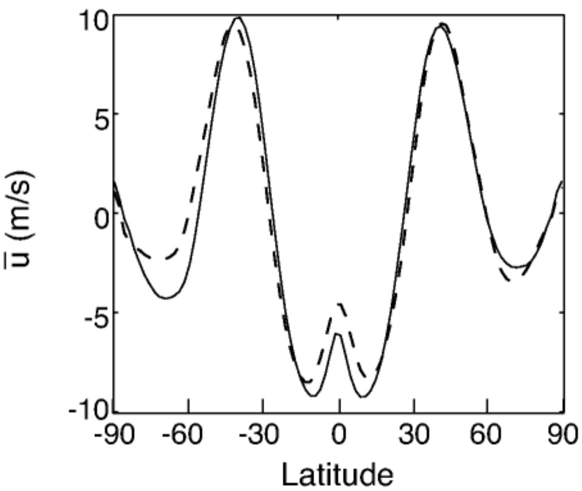

Fig. 6. Zonal-mean, time-mean surface zonal wind (m/s) in solutions with $\alpha = 1$ (solid curve) and $\alpha = 300$ (dashed).

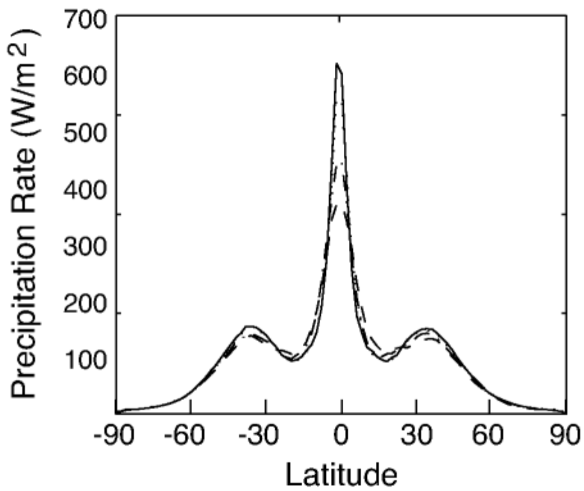

Fig. 7. Zonal-mean, time-mean precipitation rate (W/m^2) for all four climates: $\alpha = 1$ (solid), $\alpha = 100$ (dotted), $\alpha = 200$ (dot-dashed), $\alpha = 300$ (dashed).

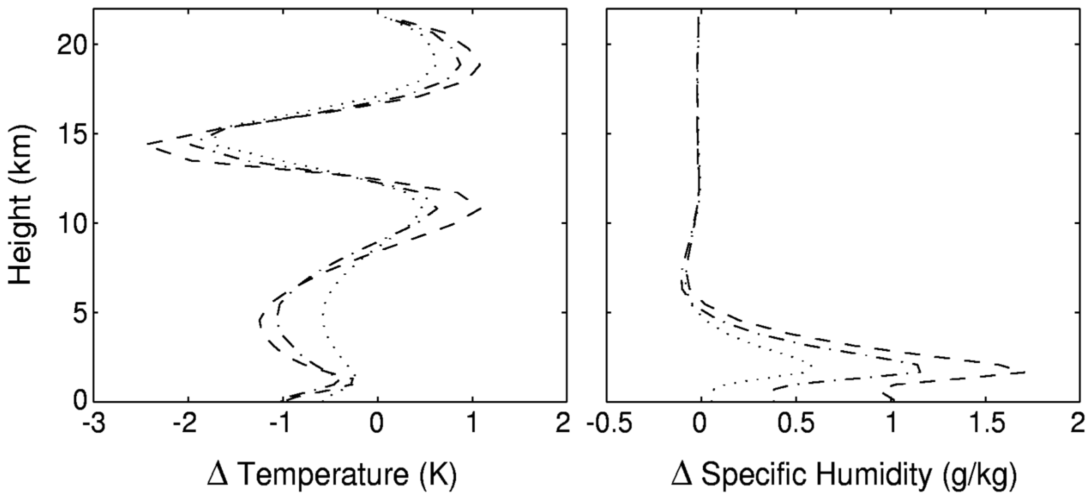

Fig. 8. Vertical profiles of time-mean temperature (K) and specific humidity (g/kg) averaged over the Tropics in the three hypohydrostatic solutions, plotted as a departure from the control climate: $\alpha = 100$ (dotted), $\alpha = 200$ (dot-dashed), $\alpha = 300$ (dashed).

Table 1:

	$\alpha = 1$	$\alpha = 100$	$\alpha = 200$	$\alpha = 300$
$\lvert \boldsymbol{V} \rvert_{\mathrm{RMS}}(40°)$	18.8	19.1	19.1	18.7
$w_{\mathrm{max}}(\mathrm{Eq})$	1.4	0.61	0.36	0.30
(35 m/s)r	1.4			
(35 m/s)$2/\alpha$		0.70	0.35	0.23

Table 1: RMS horizontal wind at ±40 deg and maximum upward velocity at the equator for the four climates determined by α, as well as estimates of vertical velocity based on simple scaling considerations. See text for the meaning of α and r.